UDK 669.14:669.112.221:536.421.4
Original scientific article/Izvirni znanstveni članek

ISSN 1580-2949
MTAEC9, 47(6)739(2013)

EFFECTS OF SOLIDIFICATION PARAMETERS ON THE MICRO- AND MACROSTRUCTURE OF THE X19CrMoVNbN11-1 STEEL

VPLIVI PARAMETROV STRJEVANJA NA MAKRO IN MIKROSTRUKTURO JEKLA X19CrMoVNbN11-1

Mitja Koležnik[1], Aleš Nagode[2], Grega Klančnik[2], Jože Medved[2], Bernarda Janet[1], Milan Bizjak[2], Ladislav Kosec[2]

[1]Metal Ravne, d. o. o., Koroška cesta 14, 2390 Ravne na Koroškem, Slovenia
[2]Faculty of Natural Sciences and Engineering, University of Ljubljana, Aškerčeva cesta 12, 1000 Ljubljana, Slovenia
mitja.koleznik@metalravne.com

Prejem rokopisa – received: 2012-11-27; sprejem za objavo – accepted for publication: 2013-04-15

Differential scanning calorimetry (DSC) of the X19CrMoVNbN11-1 steel was used for determining phase-transformation temperatures. To study the effect of the cooling rate on the shape and chemical composition of primary precipitates with SEM and EDXS, an investigation was made on DSC samples. With a decreasing cooling rate precipitates became shorter and thicker and with a higher cooling rate the contents of Nb and V increased.
The effects of solidification parameters on micro-segregations were investigated on the re-melted steel solidified at different parameters (experimental ingots). The microstructure was examined using SEM and EDXS. A higher volume fraction of segregation is present in the more rapidly cooled steel. In positive segregations the largest increase of the Cr content and a minor increase in the concentrations of Mo and V were observed. The effect of melt superheating on the columnar and equiaxed crystallization zone shares was also investigated. At higher melt temperatures a higher fraction of columnar crystals was present.

Keywords: solidification parameters, transformation temperatures, precipitate shape, segregation, melt superheating, crystallization zones

Za določitev temperatur faznih pretvorb v jeklu X19CrMoVNbN11-1 smo izvedli diferenčno vrstično kalorimetrijo (DSC). Pri vzorcih smo z vrstičnim elektronskim mikroskopom (SEM) in energijsko disperzijsko spektroskopijo rentgenskih žarkov (EDXS) preiskovali vpliv različnih hitrosti ohlajanja na obliko in kemijsko sestavo primarnih karbonitridov. Z manjšo hitrostjo ohlajanja so bili izločki krajši in debelejši. Vsebnost Nb in V v izločkih pa je naraščala z večjo hitrostjo ohlajanja.
Izdelani so bili eksperimentalni ingoti, ki so bili strjeni v različnih razmerah. Preiskovali smo vpliv razmer pri strjevanju na razsežnost izcejanja, ki smo ga ugotavljali z vrstičnim elektronskim mikroskopom in EDXS-analizo. Obseg izcejanja je bil večji pri jeklu z večjo hitrostjo ohlajanja. V pozitivnih izcejah se je najbolj povečala koncentracija Cr, v manjšem obsegu pa se je povečala tudi koncentracija Mo in V. Preiskali smo tudi vpliv pregretja taline na delež kristalizacijskih področij s stebrastimi in enakoosnimi zrni. Z višjo temperaturo pregretja taline se je povečal delež stebrastih kristalnih zrn.

Ključne besede: vpliv parametrov strjevanja, temperature premen, oblika izločkov, izcejanje, pregretje taline, kristalizacijska področja

1 INTRODUCTION

The vital parts (like the components for steam and gas turbines, steam pipes, boilers, etc.) for thermal power plants must fulfil very high quality standards. The most widely used creep-resistant steels in power plants are martensitic steels with 9 % to 12 % Cr. They have the best combination of physical and elastic properties, a high creep strength, a high resistance against thermal fatigue and a high steam-oxidation resistance.[1–5] To ensure the adequate properties the minimum structure homogeneity right from the start of a manufacturing process is necessary.

During solidification in industrial conditions, non-equilibrium conditions prevail resulting in chemical inhomogeneities on the macro- and micro-scale (macro- and micro-segregations).[6–8] Micro- or crystal segregations represent a change in the concentration of alloying elements across a grain cross-section with low melting elements on the grain boundaries. The smallest concentration of alloying elements is expected to be found in the core of dendrites. Since the mobility of atoms in the solid phase is rather small and the diffusion times are short, chemical inhomogeneities remain to room temperature. The intensity of segregations and the microstructural evolution in an as-cast sample depends on the solidification rate. Casting parameters also affect the volume fraction of individual crystallization zones in solidified ingots. The anisotropy of columnar zones can decrease the ductility of steel during a plastic deformation.[9–11]

2 EXPERIMENTAL WORK

The alloy used in this study was the creep-resistance steel X19CrMoVNbN11-1 with a typical chemical composition shown in **Table 1**. Differential scanning calorimetry was used for determining the characteristic

Table 1: Typical chemical composition of the X19CrMoVNbN11-1 steel in mass fractions, *w*/%
Tabela 1: Tipična kemijska sestava jekla X19CrMoVNbN11-1 v masnih deležih, *w*/%

C	Si	Mn	Cr	Mo	Ni	V	Nb	N	B
0.19	0.30	0.55	10.75	0.75	0.5	0.20	0.33	0.08	max. 0.0015

temperatures of solidification, using a Netzsch STA 449 C Jupiter. In **Table 2** the parameters of DSC analyses are given. DSC analyses were performed in a protective atmosphere of volume fraction 99.999 % N_2 and, as a reference, an empty corundum crucible was used. DSC specimens were also used to determine the effects of solidification parameters on the microstructure. Thermodynamic calculations were performed using the ThermoCalc program with an internal thermodynamic database, TCFE7.

Table 2: Parameters of an DSC analysis
Tabela 2: Parametri DSC-analize

sample	T_{max}/°C	$v_{heating}$ / (K min^{-1})	$v_{cooling}$/ (K min^{-1})
S1	1550	1	1
S25	1550	25	25
S6P	1600	6	6
S6	1550	6	6

Table 3: Casting parameters of experimental ingots
Tabela 3: Parametri litja eksperimentalnih ingotov

No.	m_{load}/kg	T_{mold}/°C	$T_{casting}$/°C	Mold isolation
1	11	318	1547	no
2	10.97	280	1560	yes
3	11.02	330	1690	yes
4	8.75	30	1550	no

The experimental ingots of the X19CrMoVNbN11-1 creep-resistant steel were prepared by melting the steel in an inductive vacuum furnace. The steel was solidified under different cooling conditions. To achieve different cooling rates of the castings, different preheated moulds were used. The casting parameters are shown in **Table 3** and the cooling rates of the ingots are shown in **Figure 1**.

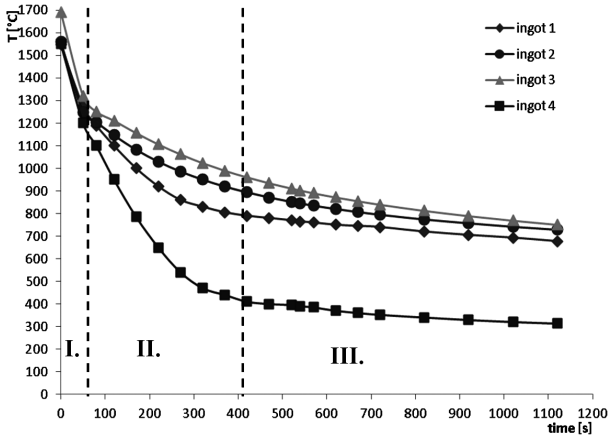

Figure 1: Cooling rates of ingots
Slika 1: Hitrost ohlajanja posameznega ingota

The samples for the investigation of the macro- and microstructure were cut from the ingots without heat treatment. For the metallographic examination of the macrostructure, the steel plates were grinded and etched in a hot 50 % HCl solution at 50 °C. The samples for the microstructural investigation were grinded, polished and etched with the Villela etchant.

The metallographic investigation of the steel was carried out on a scanning electron microscope (SEM), JEOL JSM-5610 with an energy-dispersive x-ray spectrometer (EDXS), GRESHAM Scientific Instruments, model SIRIUS 1YSUTW. The results are given as a quantitative spot (EDXS spectrum) and qualitative EDXS line profile and as mapping analyses.

2.1 Thermodynamic model for M(C, N)

In the CALPHAD approach each phase should be described with a proper thermodynamic model. In this paper emphasis is placed only on the thermodynamic modelling of M(C, N). M stands for the metals mixing on the first sublattice, sublattice #1. $M_{a1}(C, N)_{a2}$ is modelled with two sublattice models with the second sublattice representing the interstitial atoms of C and N. Va stands for vacancy. The carbonitrides present in steels can be modelled with a combination of Fe, Nb, Ti and others on the first sublattice, and C, N and Va on the second one; an example is given for $(Fe, Nb, Ti)_{a1}(C, N, Va)_{a2}$. The Gibbs free energy, G_m, of such a formula for one formula unit is described with the following equation:[12]

$$G_m = y_{Fe}y_c{}^0G_{Fe:C} + y_{Nb}y_c{}^0G_{Nb:C} + y_{Ti}y_c{}^0G_{Ti:C} +$$
$$+ y_{Fe}y_N{}^0G_{Fe:N} + y_{Nb}y_N{}^0G_{Nb:N} + y_{Ti}y_N{}^0G_{Ti:N} +$$
$$+ y_{Fe}y_{Va}{}^0G_{Fe:Va} + y_{Nb}y_{Va}{}^0G_{Nb:Va} + y_{Ti}y_{Va}{}^0G_{Ti:Va} +$$
$$+ a_1RT(y_{Fe}\ \ln y_{Fe} + y_{Nb}\ \ln y_{Nb} + y_{Ti}\ \ln y_{Ti}) +$$
$$+ a_2\ RT(y_C\ \ln y_C + y_N\ \ln y_N + y_{Va}\ \ln y_{Va}) + EG_m$$

where y_i represents the site fractions of component i on the first or second sublattice (I or II). $G^0_{i:j}$ is the Gibbs free energy where only *i* and *j* are occupying the sublattices. G^E_m represents the excess Gibbs energy. In addition, the term for magnetic contribution can also be added. For a more complex formula with more elements on the first sublattice the Gibbs energy is described below; here a_1 or a_2 represent the site occupancy:

$$G_m = \sum_i \sum_j y_i' y_j''{}^0 G_{i:j} +$$

$$+RT\left(a_1 \sum_i y_i' \ln(y_i') + a_2 \sum_j y_j'' \ln(y_j'')\right) + EG_m$$

In this study the modelling was done using the following formula for carbonitride with an fcc structure:

(Nb, Cr, Fe, Mn, Mo, Ni, Si, V)1(C, N, Va)1

where in sublattice #1 the major constituents are Nb, Cr, V and in sublattice #2 the major constituents are C and N, with Va as a minor constituent.

3 RESULTS AND DISCUSSION

Differential scanning calorimetry was used for determining transformation temperatures. The increasing heating rate influenced the phase transformation at higher temperatures and with the increasing cooling rate these transformations were moved to lower temperatures. **Table 4** shows the A_{r1} temperatures of the solidification curves.

Table 4: Phase-transformation temperatures
Tabela 4: Temperature faznih premen

sample	S1	S6	S25	S6P
T_{max}/°C	1550	1550	1550	1600
v_s/v_o	1/1	6/6	25/25	6/6
A_{r1}/°C	812	823	835	821
$T_{liquidus}$/°C	1497	1510	1462	1495
$T_{solidus}$/°C)	1492	1493	1443	1480

The metallographic investigation of DSC samples revealed that the cooling rate has a great effect on the shape and chemical composition of the precipitates. Combining the Thermo-Calc software and EDXS analysis, the precipitates were identified as Nb(C, N) with low contents of V and Mo. At the highest cooling rate of 25 K min^{-1}, the precipitates were needle shaped with a diameter of approximately 0.5 μm and a length of up to 35 μm with a faceted surface. At a lower cooling rate, the precipitates were shorter and thicker, and their surface was less faceted. At the cooling rate of 6 K min^{-1}, the diameter of the precipitates was approximately 1 μm and the length was approximately 15 μm. The precipitates formed at different cooling rates are shown in **Figures 2** and **3**. A micro-chemical analysis of the precipitates indicated that at higher cooling rates the contents of Nb and V increased **Figure 4** shows the concentration ratio of Nb and V w(Nb)/w(V) in the precipitates as a function of the cooling rate. At higher cooling rates the w(Nb)/w(V) ratio was increased indicating that, at a higher cooling rate, the content of Nb in the precipitates increased faster than the content of V.

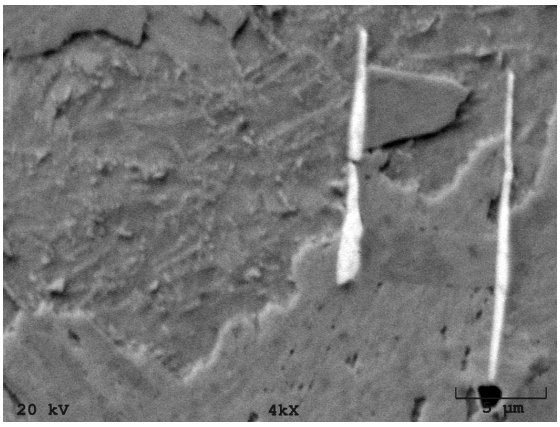

Figure 3: Shape of precipitates at 6 K min^{-1}
Slika 3: Oblika izločkov pri hitrosti ohlajanja 6 K min^{-1}

A comparison of the macro- and microstructures of the experimental ingots was made. In all the ingots three distinct crystallization zones were found. In the central region there was a zone of fine, randomly oriented, equiaxed grains and, in the outer region, a zone of columnar grains was observed. On the ingot surfaces, a zone of very fine equiaxed grains (chill crystals) was observed. The degree of melt superheating has the strongest influence on the shares of the columnar and equiaxed zones in the experimental ingots (in our case the temperatures of melt superheating and the casting temperatures from **Table 3** are equal). The smallest share of the columnar zone was found in ingot 1 with the melt heated to the lowest temperature (1547 °C). The highest share of the columnar zone was found in ingot 3 with the overheating of up to 1690 °C. **Table 5** shows the shares

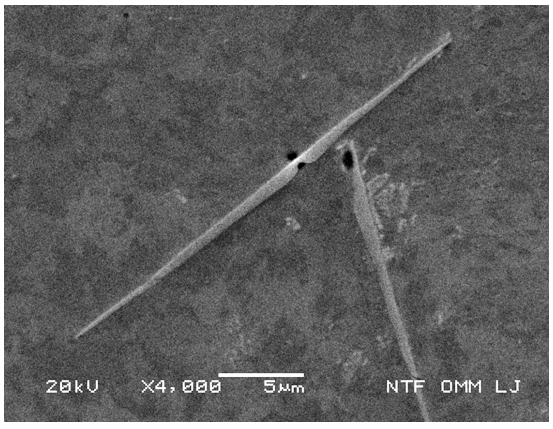

Figure 2: Shape of precipitates at 25 K min^{-1}
Slika 2: Oblika izločkov pri hitrosti ohlajanja 25 K min^{-1}

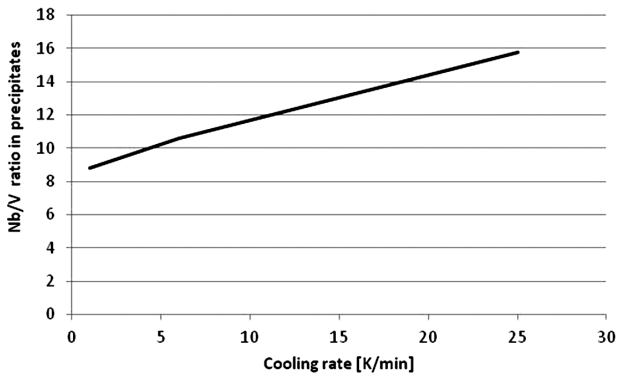

Figure 4: Concentration ratio of Nb and V in precipitates as a function of the cooling rate
Slika 4: Razmerje koncentracije Nb in V v izločkih v odvisnosti od hitrosti ohlajanja

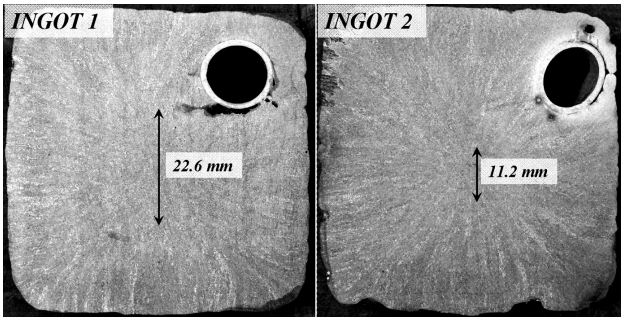

Figure 5: Equiaxed and columnar zones in ingots 2 and 3
Slika 5: Primerjava deleža področij s stebrastimi in enakoosnimi zrni v ingotih 2 in 3

of the columnar zones (w_{trans}/%) in each ingot. In **Figure 5** a comparison of the macrostructures of ingots 2 and 3 can be observed together with the corresponding diameters of the equiaxed zones. At a higher degree of melt superheating more heterogeneous nuclei dissolve. The smaller is the concentration of heterogeneous nuclei in a melt, the higher the degree of supercooling that is needed for the solidification to start. A higher degree of supercooling increased the share of the columnar zone in a solidified ingot.

Table 5: Share of the columnar zone in ingots
Tabela 5: Delež področja stebrastih zrn v posameznem ingotu

	ingot 1	ingot 2	ingot 3	ingot 4
$T_{casting}$/°C	1547	1560	1690	1550
w_{trans}/%	88.9	90.7	95.5	89.9

The cooling curves of experimental ingots are shown in **Figure 1**. It can be seen that every curve shows three distinct regions. Region I with the highest slope represents a very intense cooling of the ingots immediately after casting when the melt comes into contact with the wall of the colder metallic mold. However, the steepest slope shows ingot 3 with the highest casting temperature. In region II the cooling rates slow down due to the generated crystallisation heat. In this region the cooling rates depend on the casting parameters (the mold temperature and the mold isolation) (**Table 3**). In this region, the highest drop in the temperature is observed for ingot 4 with the coldest mold (not preheated) and without isolation. In region III with the stationary cooling having the lowest cooling rates, a small difference in the slopes of the cooling curves are found except for ingot 4 with an unpreheated mold and without isolation. In all the investigated ingots crystal segregations were observed with the segregation intensity (the volume fraction) depending on solidification parameters. The most intense segregation was found in ingot 4, cast in a cold mold (the highest cooling rate). The least intense segregation was found in ingot 2, cooled with the lowest rate. In the region with the maximum and minimum contents of alloying elements, a micro-chemical analysis was carried out. In **Figure 6** the EDXS micro-chemical analysis of

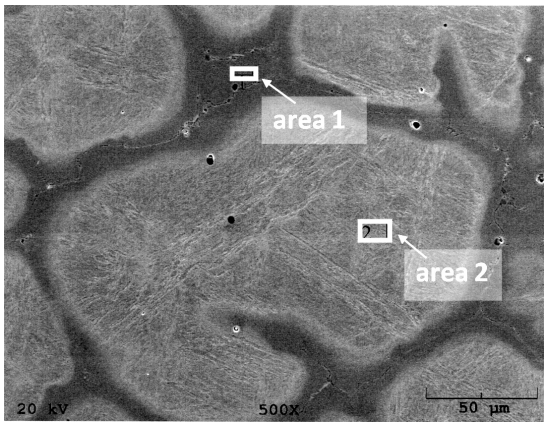

Figure 6: EDXS analyis of the microstructure of ingot 4. Chemical compositions of areas 1 and 2 are in **Table 6**. The darker area – higher contents of alloying elements.
Slika 6: Mikrokemijska analiza (EDXS) ingota 4. Kemijska sestava področja 1 in področja 2 je podana v **tabeli 6**. Temnejša območja – povečana koncentracija zlitinskih elementov.

Table 6: Chemical composition (EDXS analysis) of segregations in mass fractions, *w*/%; see also **Figure 6**
Tabela 6: Kemijska sestava (EDXS-analiza) izcej v masnih deležih, *w*/%; glej **sliko 6**

	Fe	Si	Cr	Mn	Mo	Ni	V	Nb
Area 1	84.45	0.29	13.10	0.32	0.66	0.62	0.29	0.27
Area 2	89.24	0.26	9.03	0.36	0.42	0.48	0.18	0.03

ingot 4 is presented and the chemical composition of the selected areas is given in **Table 6**. Differences in the chemical composition affect the intensity of etching. Darker areas on **Figure 6** are positive segregations with higher chromium contents. The concavity of positive segregations indicates that they were solidified last with the formation of one carbide eutectic with the lowest melting point (**Figure 7**). The largest variation between the alloying elements was measured for the concentration of Cr. The difference between the maximum and minimum Cr contents was much more explicit for the rapidly cooled ingot. For ingot 2 the difference in the concentration of Cr was approximately 2.5 % and for

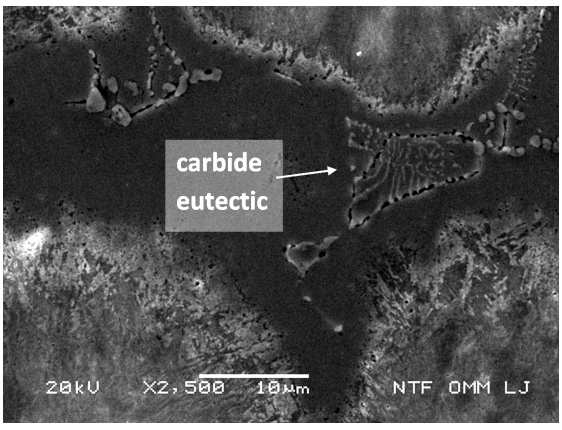

Figure 7: Positive segregations with carbide eutectic
Slika 7: Pozitivne izceje s karbidnim evtektikom

ingot 4 the difference was approximately 4 % (mass fractions). The segregation of Cr in each ingot was characterised with the segregation index I_s (1) and segregation rate I_{sg} (2):

$$I_s = \frac{C_{max}}{C_{min}} \quad (1)$$

$$I_{sg} = \frac{C_{max} - C_{min}}{C_0} \quad (2)$$

where C_{max} is the maximum, and C_{min} is the minimum content, while C_0 is the average content of Cr in each ingot. The results are shown in **Table 7**. The concentrations of V and Mo were also increased in positive segregations.

Table 7: Mass index and level of the Cr segregation in ingots
Tabela 7: Masni indeks ter stopnja izcejanja Cr za posamezen ingot

	C_{max}/%	C_{min}/%	C_0/%	I_s	I_{sg}/%
ingot 1	11.12	9.47	9.98	1.17	16.54
ingot 2	12.88	10.41	10.24	1.24	24.44
ingot 3	11.83	10.10	10.10	1.17	17.12
ingot 4	13.10	9.03	10.02	1.45	40.63

The change in the concentration of the alloying elements in the dendrite cross-section was determined with the qualitative EDXS line analysis of ingot 4 in **Figure 8**. The line intersects one positive segregation in two areas (between 20–40 μm and between 56–68 μm along with the carbide at approximately 62). There is a significant increase in the concentrations of Cr and Mn and a minor increase in the concentrations of V in the areas of positive segregation. At the carbide intersection, a large increase in the carbide-forming elements, like Nb, Mo and V, is present. In the microstructure in **Figure 8** carbide eutectic is also presented. In **Figure 9** a qualitative mapping analysis of carbide eutectic is shown, indicating increased contents of Mo, Nb and V like for the carbide in the line analysis from **Figure 8**.

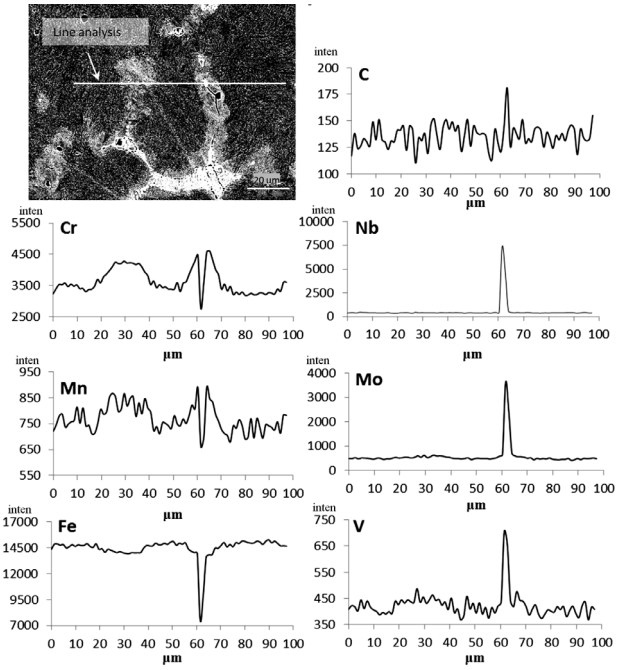

Figure 8: Qualitative EDXS line analysis of ingot 4
Slika 8: Kvalitativna črtna EDXS-analiza ingota 4

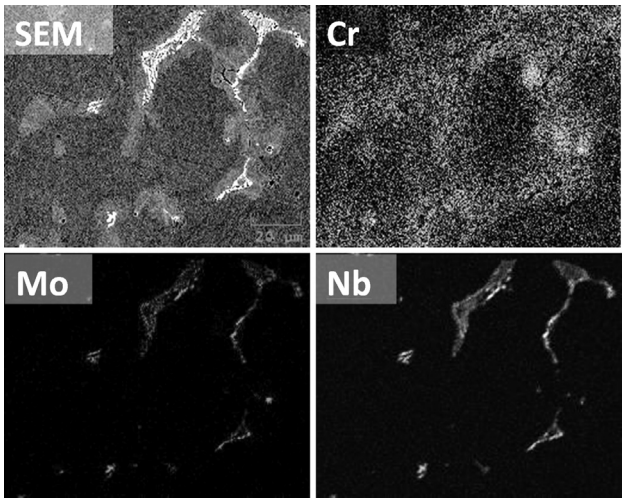

Figure 9: Qualitative EDXS mapping analysis of the segregations with carbide eutectic
Slika 9: Kvalitativna ploskovna EDXS-analiza izcej s karbidnim evtektikom

4 CONCLUSIONS

To determine the influence of solidification parameters, the macro- and microstructure as well as the chemical homogeneity of the creep-resistant steel of grade X19CrMoVNbN11-1 were investigated.

- The heating and cooling rates affect the solidification interval. By increasing the heating rate, the solidification interval is shifted to a higher temperature, while with a higher cooling rate the solidification interval is shifted to a lower temperature.
- The cooling rate affects the shape and chemical composition of precipitates. At the higher cooling rates the precipitate shapes were long faceted needles, and at a lower cooling rate the precipitates were shorter and thicker. They were identified as the Nb(C, N)-type precipitates.
- At the higher cooling rates the contents of Nb and V were higher.
- The degree of melt overheating influenced the respective proportions of columnar and equiaxed zones. With higher melt superheating the share of the columnar zones increases.
- At a higher cooling rate the intensity of segregation and the intensity of positive segregations of Cr were greater.
- In the investigated steel the last solidified melt had a eutectic composition.

5 REFERENCES

[1] A. Nagode, L. Kosec, B. Ule, G. Kosec, Review of creep resistant alloys for power plant applications, Metalurgija, 50 (**2011**) 1, 45–48

[2] F. Vodopivec, D. A. Skobir, M. Jenko, B. Žužek, M. Godec, Nucleation and growth of $M_{23}C_6$ particles in high-chromium creep resistant steel, Mater. Tehnol., 46 (**2012**) 6, 633–636

[3] D. Rojas Jara, 9–12 % Cr heat resistant steels: Alloy design, TEM characterisation of microstructure evolution and creep response at 650 °C, Fakultät für Maschinenbau der Ruhr, Universität Bochum, 2011

[4] R. L. Klueh, R. H. Donald, High-Chromium Ferritic and Martensitic Steels for Nuclear Applications, ASTM International, (**2001**), 5–27

[5] F. Abe, T. Kern, R. Viswanathan, Creep-resistant steels, Woodhead Pub. Ltd, Cambrige, England 2008

[6] W. Kurz, D. J. Fisher, Fundamentals of solidification, Trans Tech Publications Ltd, Aedermannsdorf 1986

[7] University of Cambridge, Casting: Microstructure and segregation in castings [online]. 2004, [cited 2012-07-26]. Available from World Wide Web: http://www.doitpoms.ac.uk/tlplib/casting/microsegregation.php

[8] S. Spaić, Fizikalna metalurgija: zgradba kovinskih materialov, strjevanje kovinskih zlitin, Naravoslovnotehniška fakulteta, Univerza v Ljubljani, Ljubljana 2002

[9] M. Durand-Charre, Microstructure of Steels and Cast Irons, Springer, Paris 2003

[10] J. W. Elmer, S. M. Allen, T. W. Eagar, Microstructural development during solidification of stainless steel alloys, Metallurgical transactions, 20 (**1989**), 2117–2131

[11] H. Biloni, W. J. Boettinger, Solidification, In: R. W. Chan, P. Haasen (eds.), Physical Metallurgy, Elsevier Science BV, Amsterdam 1996, 670–842

[12] B. J. Lee, Thermodynamic Assessment of the Fe-Nb-Ti-C-N System, Metallurgical and Materials Transactions A, 32 (**2001**), 2423–2439